AD NUMBER
AD317028
CLASSIFICATION CHANGES
TO: **UNCLASSIFIED**
FROM: **SECRET**
LIMITATION CHANGES
TO: **Approved for public release; distribution is unlimited. Document partially illegible.**
FROM: **Distribution authorized to U.S. Gov't. agencies and their contractors; Administrative/Operational Use; MAY 1960. Other requests shall be referred to Arnold Engineering Development Center, Arnold AFB, TN. Document partially illegible.**
AUTHORITY
1 Nov 1970 Bulletin 70-21 Doc markings ; AEDC ltr 25 Dec 1970

AEDC-TN-60-84

SECRET

DOCUMENT NO. 2210
This is copy number 23
of 33, which consists of
27 pages, series A.

(TITLE UNCLASSIFIED)

FORCE TESTS ON TEN LENTICULAR MODEL CONFIGURATIONS AT MACH NUMBERS 3 AND 5 AND ANGLES OF ATTACK FROM 0 TO 90 DEG

By

A. Anderson

VKF, ARO, Inc.

May 1960

ARNOLD ENGINEERING DEVELOPMENT CENTER

AIR RESEARCH AND DEVELOPMENT COMMAND

US AF

SECRET

(Title Unclassified)

FORCE TESTS ON TEN LENTICULAR MODEL CONFIGURATIONS AT MACH NUMBERS 3 AND 5 AND ANGLES OF ATTACK FROM 0 TO 90 DEG

By

A. Anderson

VKF, ARO, Inc.

May 1960

ARO Project No. 311037

Contract No. AF 40(600)-800

ABSTRACT

Force and moment coefficients were obtained on ten lenticular configurations at Mach numbers 3 and 5 over an angle-of-attack range of 0 to 90 deg. For most of these configurations the maximum lift coefficient occurred at an angle of attack between 45 deg and 50 deg. With the models aligned normal to the flow, drag decreased as the curvature of the model surface increased.

CONTENTS

TABLES

ILLUSTRATIONS

Figures

NOMENCLATURE

C_D	Drag coefficient, drag/qS
C_L	Lift coefficient, lift/qS
C_m	Pitching-moment coefficient, pitching moment/qSc (see Figs. 2 and 3 for moment reference point)
C_N	Normal-force coefficient, normal force/qS
c	Model diameter (based on basic circular planform)
M_∞	Mach number
p_o	Stilling chamber pressure, psia
q_∞	Free-stream dynamic pressure, psia
Re/in.	Unit Reynolds number
S	Model planform area (basic circular planform)
α	Angle of attack, deg

INTRODUCTION

At the request of the Air Proving Ground Center (APGC), Eglin Air Force Base, tests were conducted on ten lenticular body configurations at Mach numbers 3 and 5 in the 12-in. tunnel (Tunnel E-1) of the von Karman Gas Dynamics Facility, AEDC, from December 28, 1959, to January 8, 1960.

These tests were made in support of APGC proposals for re-entry and target bodies of lenticular derivation. During previous tests on lenticular models in Tunnel E-1, which were made for an APGC air-borne missile proposal, longitudinal stability data at angles of attack up to 15 deg were obtained for various body configurations (Refs. 1 and 2). The objectives of the present tests were to extend the data obtained on eight of these configurations through angles of attack up to 90 deg, and to obtain comparable data on two additional lenticular configurations which had not been tested previously.

APPARATUS

WIND TUNNEL

Tunnel E-1 is an intermittnet, supersonic wind tunnel with a 12-in. square test section (Fig. 1). The top and bottom walls are flexible plates, which are manually positioned with screw jacks to produce Mach numbers ranging from 1.5 to 5. Stagnation pressures from sub-atmospheric to four atmospheres are automatically regulated by throttling the flow from a high-pressure, dry-air storage tank. Radiant coils about the storage tank provide stagnation temperatures between 70 and 120°F depending upon testing conditions. A large vacuum sphere coupled to the wind tunnel diffuser permits operation at low density levels. The angle-of-attack sector, which pitches the model in the horizontal plane, covers a range from about -5 to 15 deg.

MODELS

Ten basic lenticular configurations were tested using seventeen models. Each configuration, except 4, 5, and 16, comprised a standard series model for low angles of attack and a smaller (A-series) model for the high angles ($\alpha \geq 40°$). No A-series models were available for configurations 4 and 5, nor was there a standard model for configuration 16. The standard models

Manuscript released by author April 1960.

(Fig. 2) were 8 in. in diameter except for model 10, which was 8.258 in. in diameter. The A-series models (Fig. 3) were 3.5 in. in diameter except model 11A, which was 3.39 in. in diameter.

Model 6 had all flaps set at 0 deg (see Fig. 2); on the small model, however, (6A, Fig. 3) only the lower surface flaps were simulated since the flaps on the leeward surface are shielded by the body at high angles of attack. The tail booms of model 7A were shortened as shown in Fig. 3 for angles of attack from 70 to 90 deg. The standard model 7 was tested with all four wedges located on the tail-booms as shown in Fig. 2.

Sketches of the model and balance arrangements are given in Fig. 4. For testing at angles of attack between 0 and 15 deg the standard models were mounted on a straight sting (Fig. 4a), and for angles between 15 and 40 deg, they were supported on a 20-deg bent sting (Fig. 4b). For angles between 40 and 90 deg, the A-series models were mounted on a straight sting attached dorsally at the mid-length of the models by a socket piece which was pre-set at initial angles of attack, relative to the balance, of 45 and 75 deg (Fig. 4c). This figure also shows the shroud used to shield the balance from air forces. The balance locknut cavity on the standard models (see Fig 4a) was filled with cotton wool and faired over with dental plaster.

Selected model photographs are given in Fig. 5. Photographs of models 1 and 3 are not shown since they were identical to model 10, differing only in thickness ratio. Similarly, the A-series models 1A and 10A are adequately represented by the picture shown of model 3A.

The models, which were fabricated from aluminum, and the stings were furnished by APGC.

INSTRUMENTATION

The force and moments measurements were made with a VKF internal balance, which has design loads of ±70-lb normal force, ±190-in.-lb pitching moment, and 130-lb axial force. Outputs from the various items of instrumentation were processed on an ERA 1102 computer and the test results were made available while the test was in progress.

TEST PROCEDURE

Data were obtained for the models and angles of attack shown in Table 1. The limited angle-of-attack range ($15° < \alpha < 25°$) obtained with the standard models on the bent sting at Mach number 5 was due to tunnel choking. Because of this, no tests were made with the bent sting at Mach number 3.

The test conditions at each Mach number and angle-of-attack range are listed below. The stagnation pressure was reduced during tests with the bent sting ($15° < \alpha < 25°$) to prevent overloading the balance. The stagnation temperature varied within ± 10 of 80°F for all the tests.

Mach No.	α, deg	p_o, psia	Re/in. x 10^{-6}
3	0 - 15	15	0.2
	40 - 90	15	0.2
5	0 - 15	40	0.2
	15 - 25	20	0.1
	40 - 90	40	0.2

Pitching moments were transferred to the body mid-chord (see model sketches, Figs. 2 and 3), and the normal force and axial force were resolved to the wind axes. No base pressure measurements were made. However, measurements made of the base cavity drag during previous tests on the standard models were about one percent of the body minimum drag. The angle of attack was corrected for deflection of the balance and sting support.

The tunnel choking obtained with the standard models mounted on the bent sting is typified by the schlieren picture (Fig. 6) of Model 7 at an angle of attack of about 20 deg. Also presented are typical schlieren photographs of the models at M_∞ = 3 and 5.

PRECISION OF DATA

The uncertainties in the basic flow measurements, listed below, were taken from the tunnel airflow calibration data and the known precision of pressure measuring instrumentation.

M_∞	p_o psia	q_∞ psia
3.00	±.03	±.022
5.01	±.06	±.010

The variation in test section Mach number along the tunnel centerline was within ±0.01, and the estimated accuracy of the sector positioning of the angle of attack was ±0.1 deg.

Because of the wide range in magnitude of the forces on all the models, the accuracy with which the final coefficients were obtained varied with angle-of-attack range. Based upon the balance calibration data, the

uncertainties in the coefficients, in the ranges of angles of attack noted, were estimated to be:

α, deg	C_L		C_D		C_m	
	$M_\infty = 3$	$M_\infty = 5$	$M_\infty = 3$	$M_\infty = 5$	$M_\infty = 3$	$M_\infty = 5$
0 - 15	±. 001	±. 002	±. 0007	±. 0015	±. 0007	±. 0014
15 - 25	-	±. 004	-	±. 003	-	±. 0028
40 - 90	±. 005	±. 010	±. 012	±. 024	±. 009	±. 017

RESULTS

Since the data trends observed at both Mach numbers were identical, only the Mach number 5 data are presented. In Table 2, however, values of the maximum lift and drag coefficients and the angle-of-attack range for maximum lift are shown for each configuration at both Mach numbers. No data are given for configurations 4 and 5 since the previous data on these configurations (Ref. 1) were extended by only five degrees.

The coefficients of lift, drag, and pitching moment for each configuration at Mach number 5 are shown plotted against angle of attack in Fig. 7. With the exception of configurations 6 and 14 the data presented at angles of attack up to 15 deg were taken from Refs. 1 and 2. These referenced data are also identified by a model number because the configuration notation used in the previous tests was different from that employed here.

Referring to the plots in Fig. 7, the general trends of the data with angle of attack are the same for all configurations. Values of the maximum lift coefficient, $C_{L_{max}}$, varied from a high of 0.83 obtained on configuration 14 at an angle of attack of about 42 deg to a low of 0.58 obtained on configuration 10 at an angle of about 46 deg. On all the configurations, except 14, $C_{L_{max}}$ occurred at angles of attack between 46 and 49 deg. In the angle-of-attack range from 50 to 90 deg a decrease in lift to negative values was produced by Models 6, 7, and 16 and by the wedgeshaped configuration 14. The angle of attack at which $C_L = 0$ on configuration 14 is approximately that at which the windward surface of the model is normal to the flow.

The drag coefficients obtained with the models aligned normal to the flow varied from 1.50 to 1.65 for configurations 11 and 14, respectively. For the models with continuous surface curvature (1, 3, 10, 11, and 14), these data show that drag decreased as the curvature of the model surface increased.

With the exception of configuration 14 which was essentially neutrally stable, all the configurations are statically unstable at angles of attack up to about 40 or 45 deg. With further increase in angle of attack these nose-up pitching moments decreased as the model surfaces became more nearly normal to the flow. Additional nose-down pitching moments were produced by the rearward surfaces of configurations 6, 7, and 16, which gave significant reductions in the trim angles of attack.

The data obtained on model 14 at Mach 5 and angles of attack up to 16 deg are shown in Fig. 8. This configuration unlike the lenticular configurations previously tested for APGC (all were unstable) was essentially neutrally stable without flaps. The stability margin was about 2 percent of the chord $\left[(dCm/dC_N)_{\alpha = 0^\circ} = -0.02\right]$ with flaps. These data also show that the Reynolds numbers of these tests had no effect upon either lift or pitching moment and only a small effect upon drag at angle of attack.

Unaccounted for are the unknown effects of the sting support on the flow over the lee side of the small models. In particular, in the angle-of-attack range from 40 to 60 deg the leeward flow interacted with the model support (ahead of the balance shroud) to the extent shown in the schlieren pictures of these models at 45-deg angle of attack given in Fig. 6.

CONCLUSIONS

Test results on these configurations at Mach number 5 and high angles of attack show that

1. Peak lift coefficients ranged from about 0.58 to 0.83 and for most configurations occurred at an angle of attack between 46 and 50 deg.
2. With the model surfaces normal to the flow, drag coefficients up to 1.65 were obtained, and drag decreased as the curvature of the model surface increased.

REFERENCES

1. Anderson, A. "Stability Tests of Three Lenticular Models at Supersonic Speeds." AEDC-TN-59-99, September 1959. (SECRET)
2. Anderson, A. "Stability and Control Characteristics of Seven Lenticular Models at Mach Number 5." AEDC-TN-59-162, January 1960. (SECRET)

TABLE 1

TEST CONFIGURATION SUMMARY

CONFIG.	MODEL	M	α RANGE, DEG
1	1 1A	5 3,5	15 - 25 40 - 90
3	3 3A	5 3,5	15 - 23 40 - 90
4	4	5	15 - 25
5	5	5	15 - 25
6	6 6A	3 5 3,5	0 - 11 0 - 17 40 - 90
7	7 7A	5 3 5	15 - 18 40 - 60 40 - 90
10	10 10A	5 3,5	15 - 20 40 - 90
11	11 11A	5 3.5	15 - 20 40 - 90
14	14(Flaps) 14(No Flaps) 14A	3 5 3,5 3,5	-1 - 8 -1 - 15 -1 - 16 40 - 90
16	16A	3,5	40 - 90

TABLE 2

DATA SUMMARY

Config.	M = 5			M = 3		
	$C_{L_{max}}$	α at $C_{L_{max}}$ Deg	$C_{D(\alpha=90°)}$	$C_{L_{max}}$	α at $C_{L_{max}}$ Deg	$C_{D(\alpha=90°)}$
1	.69	46-48	1.60	.75	46-49	1.69
3	.69	46-50	1.60	.75	46-49	1.67
6	.77	46-48	1.62	.82	44-46	1.67
7	.775	49-51	1.64	-	-	-
10	.58	46-49	1.55	.64	45-47	1.62
11	.59	48-50	1.50	.63	46-48	1.57
14	.83	41-43	1.65	.88	39-41	1.70
16	.68	44-48	1.60	.73	43-46	1.65

Note: On configuration 14 the model surface is normal to the flow at about α = 84 deg.

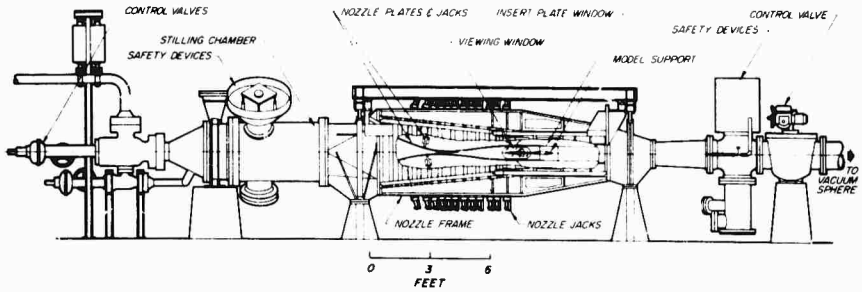

Assembly

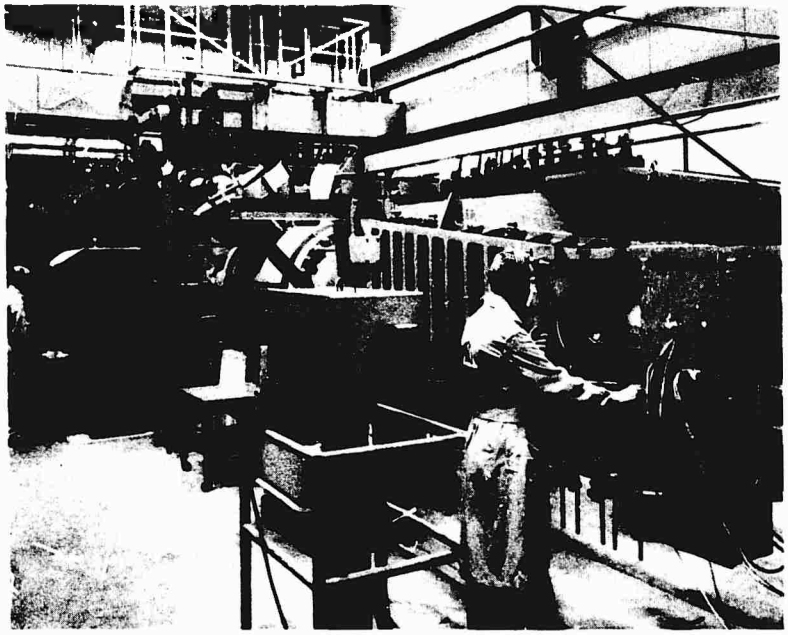

Nazzle and Test Section

Fig. 1 Tunnel E-1, a 12 x 12-in. Supersonic Wind Tunnel

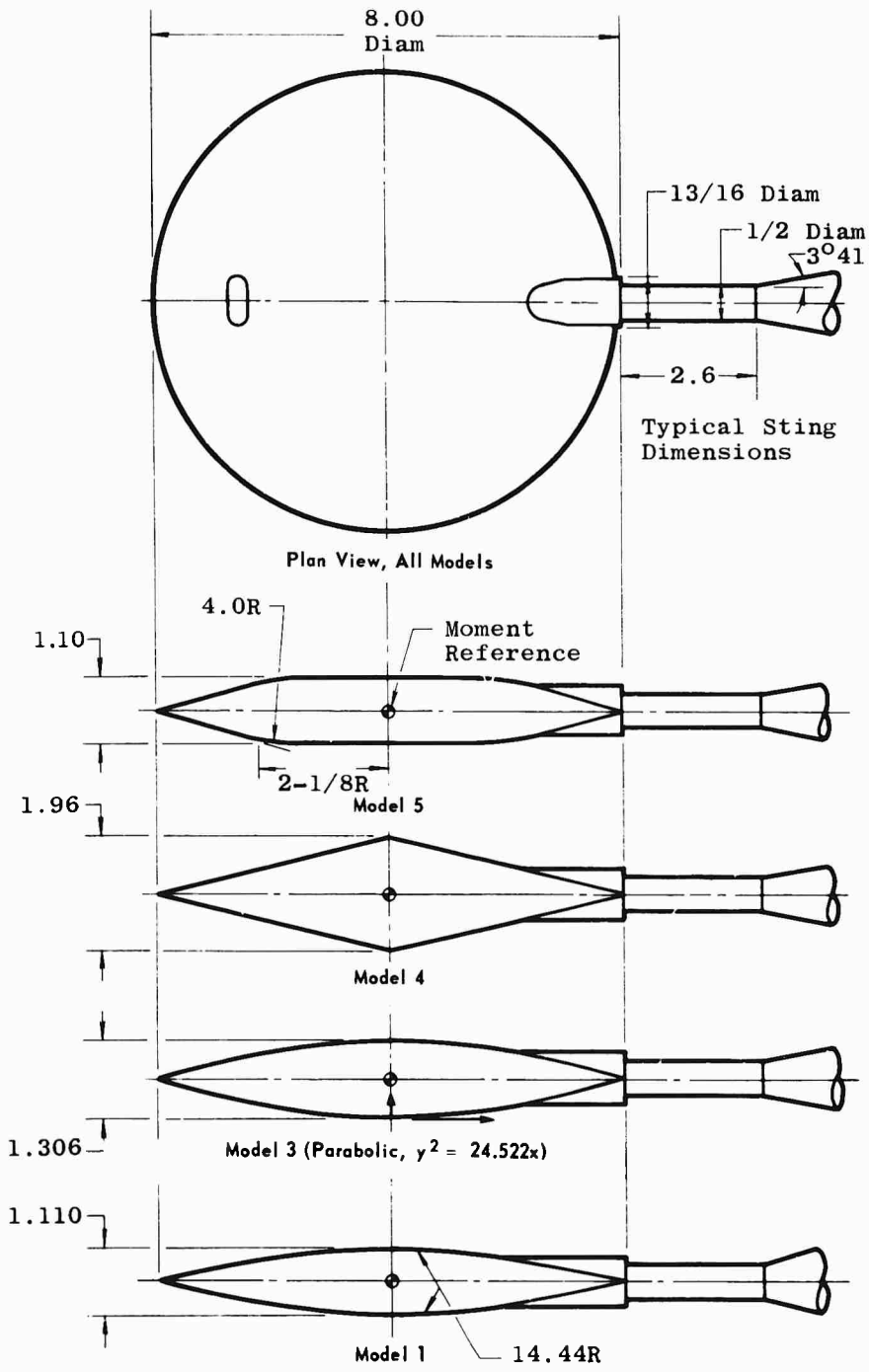

Fig. 2 Detoils of Stondard Models

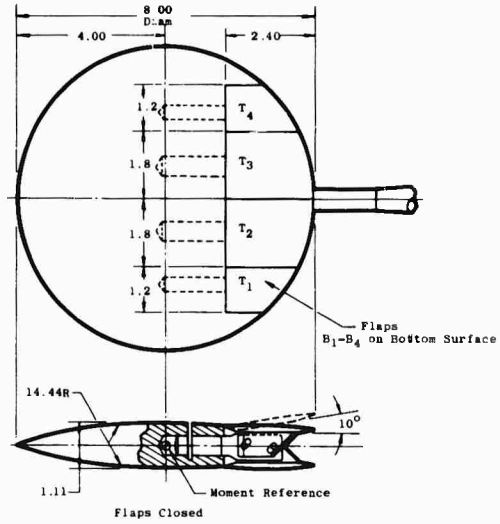

Model 6

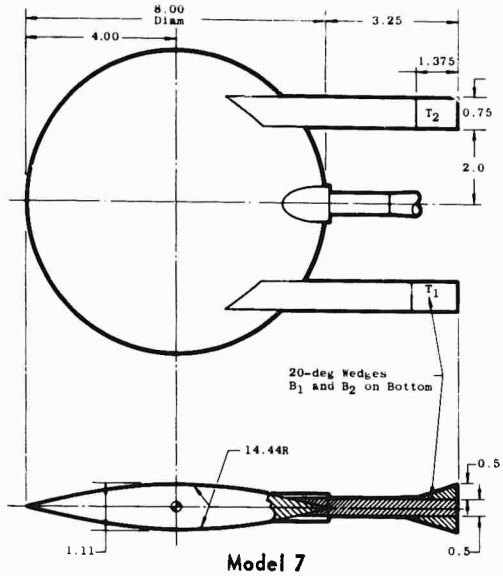

Model 7

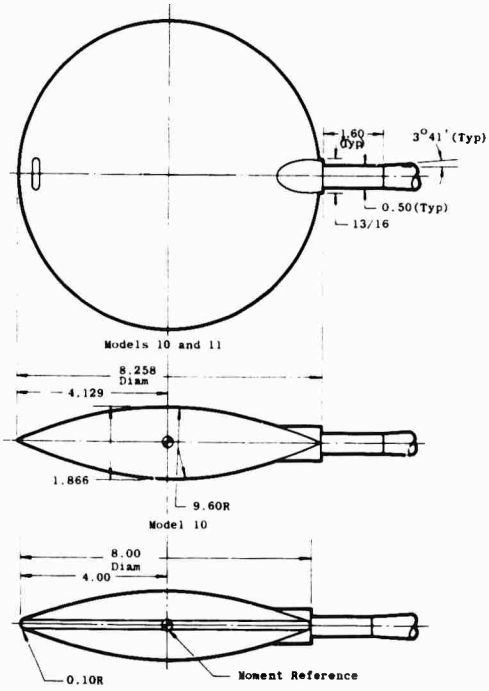

Model 11

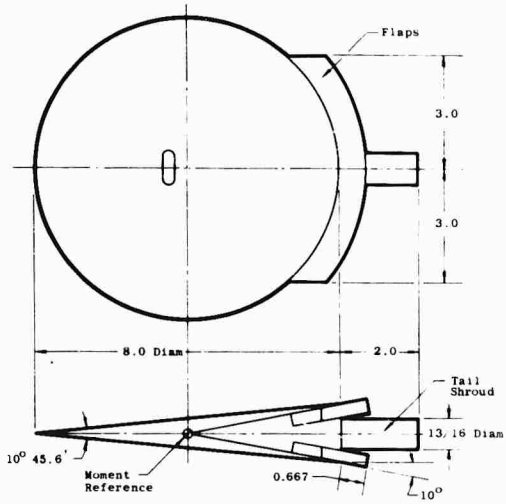

Model 14

All Dimensions in Inches

Fig. 2 Concluded

All Dimensions in Inches

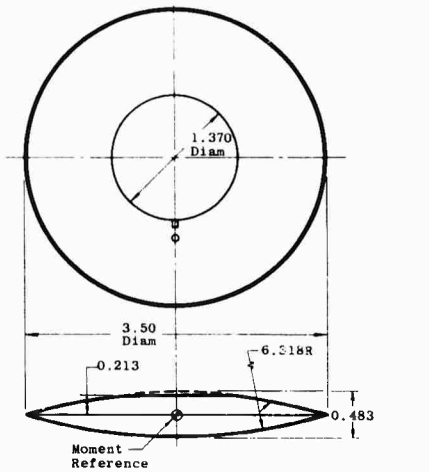

Model 1A

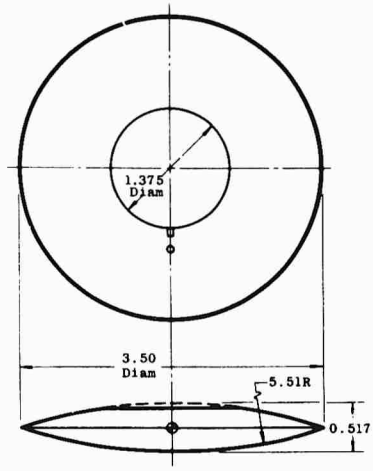

Model 3A

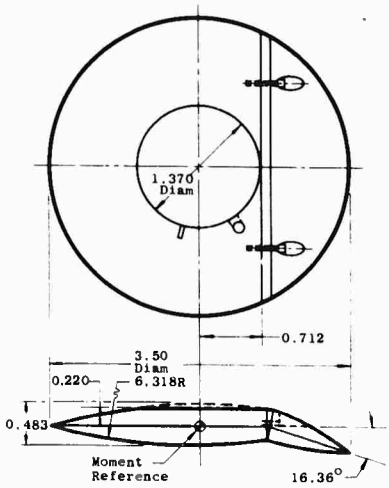

Model 6A

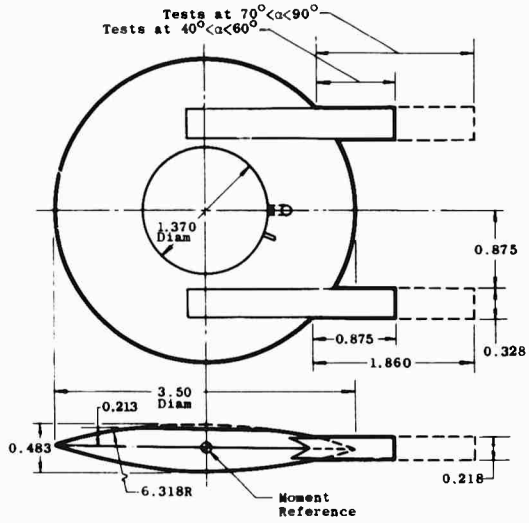

Model 7A

Fig. 3 Details of A-Series Models

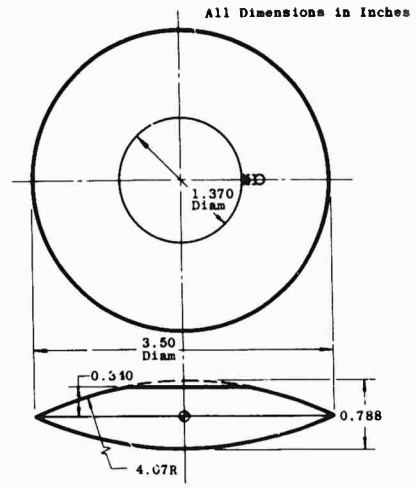

Model 10A

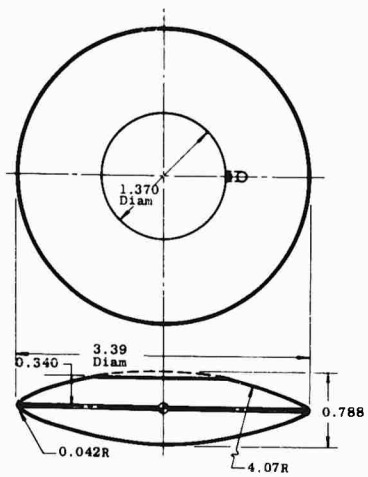

Model 11A

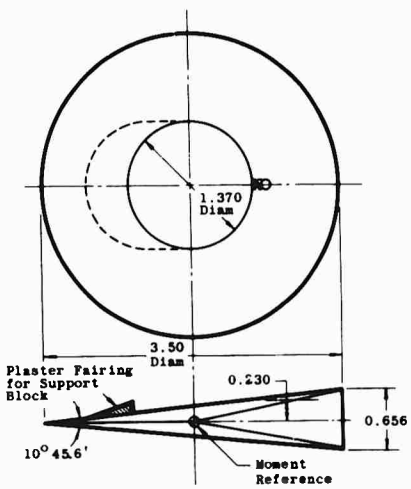

Model 14A

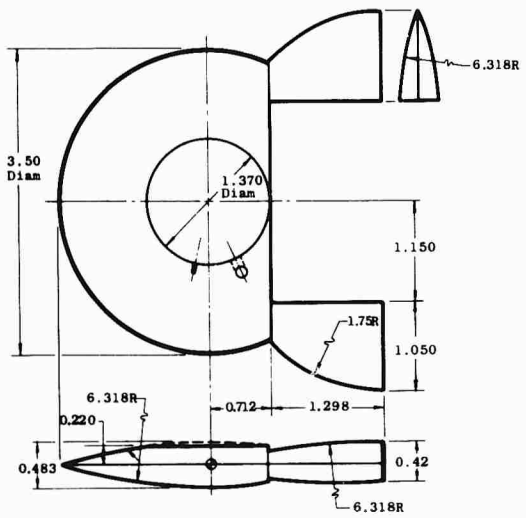

Model 16A

Fig. 3 Concluded

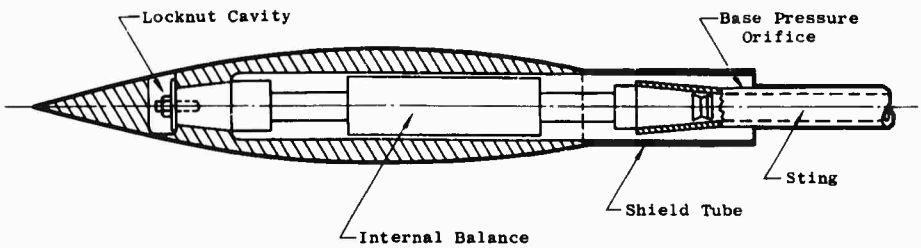

a. $-5° < \alpha < 15°$

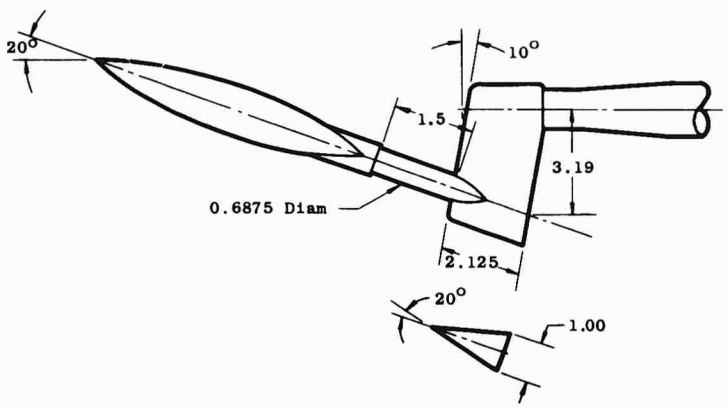

b. $15° < \alpha < 40°$

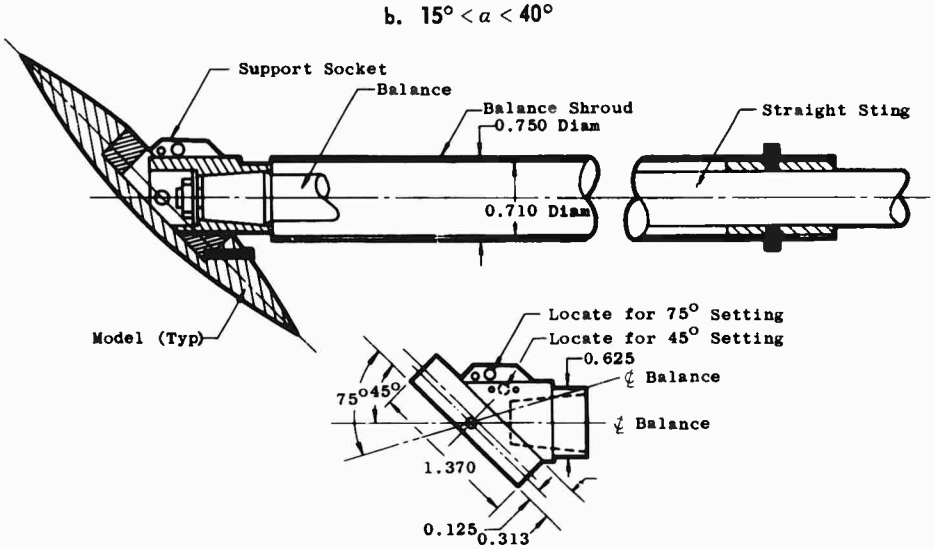

c. $40° < \alpha < 90°$

Fig. 4 Model Sting-Support Sketches

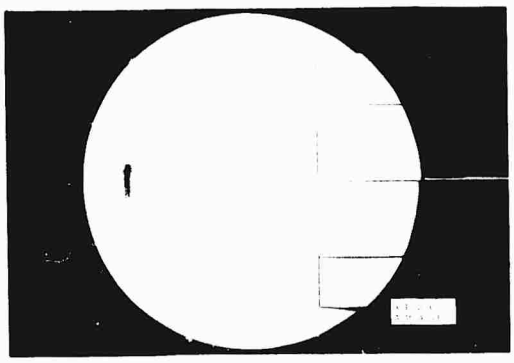

Plan View

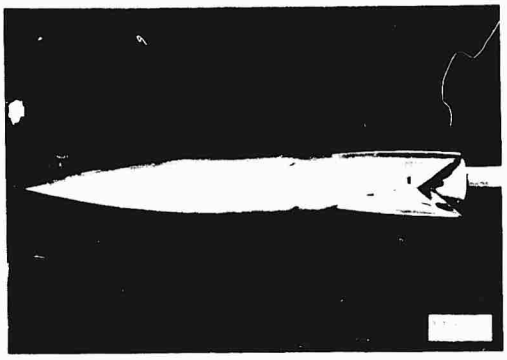

Model 6

Side View

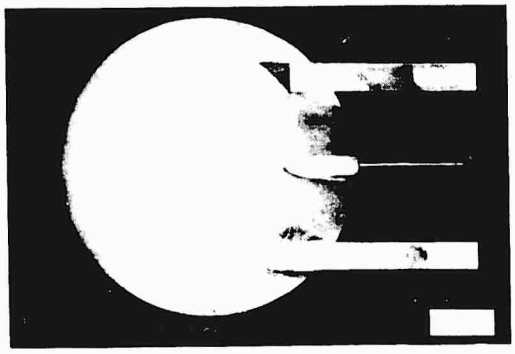

Model 7

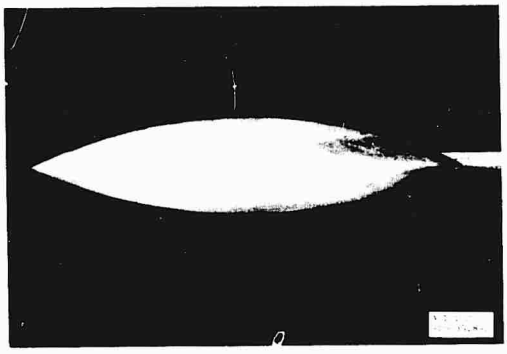

Model 10

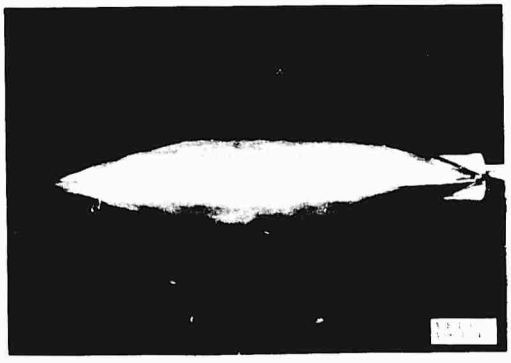

Model 11

Model 14, without Flops

Fig. 5 Model Photographs

Model 3A

Model 6A

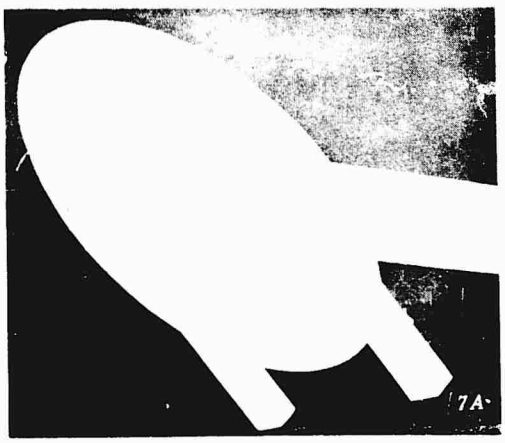

Model 7A

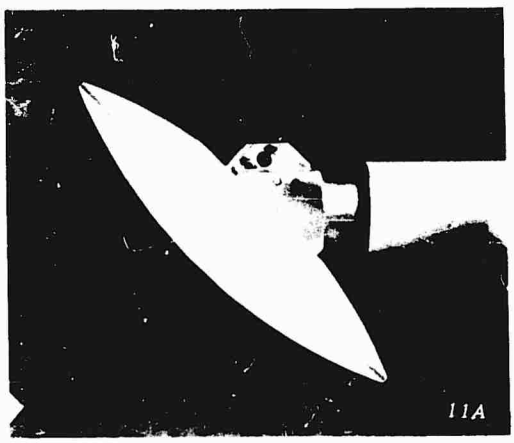

Model 11A

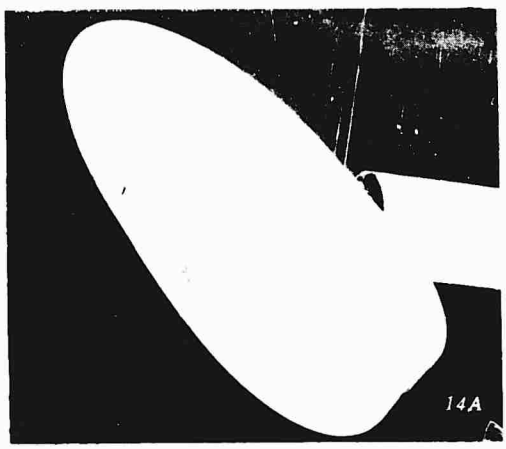

Model 14A

Model 16A

Fig. 5 Concluded

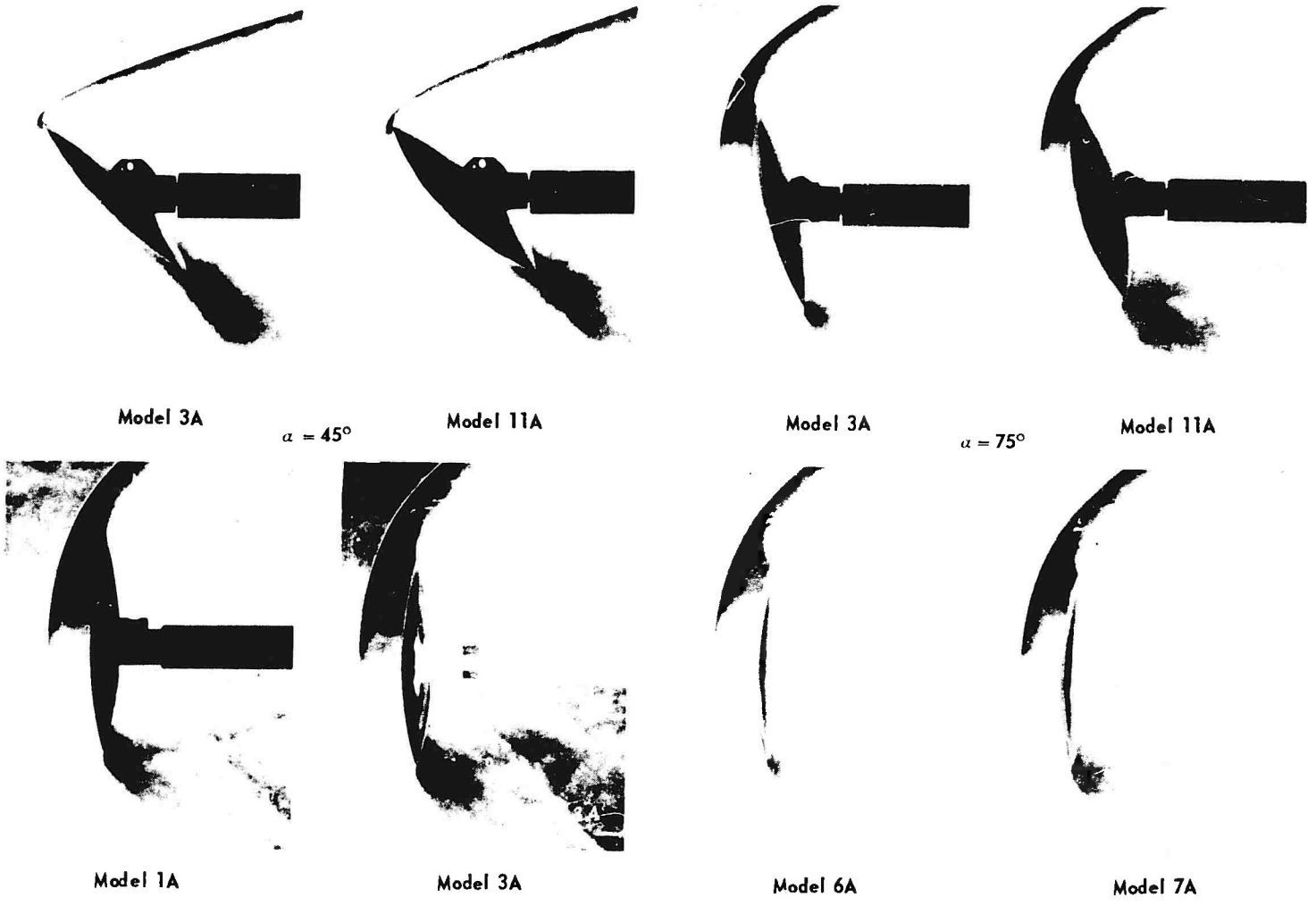

M = 5, $\alpha = 90°$

Fig. 6 Typical Schlieren Photographs

Model 11A Model 14A Model 16A

M = 5, $\alpha = 90°$

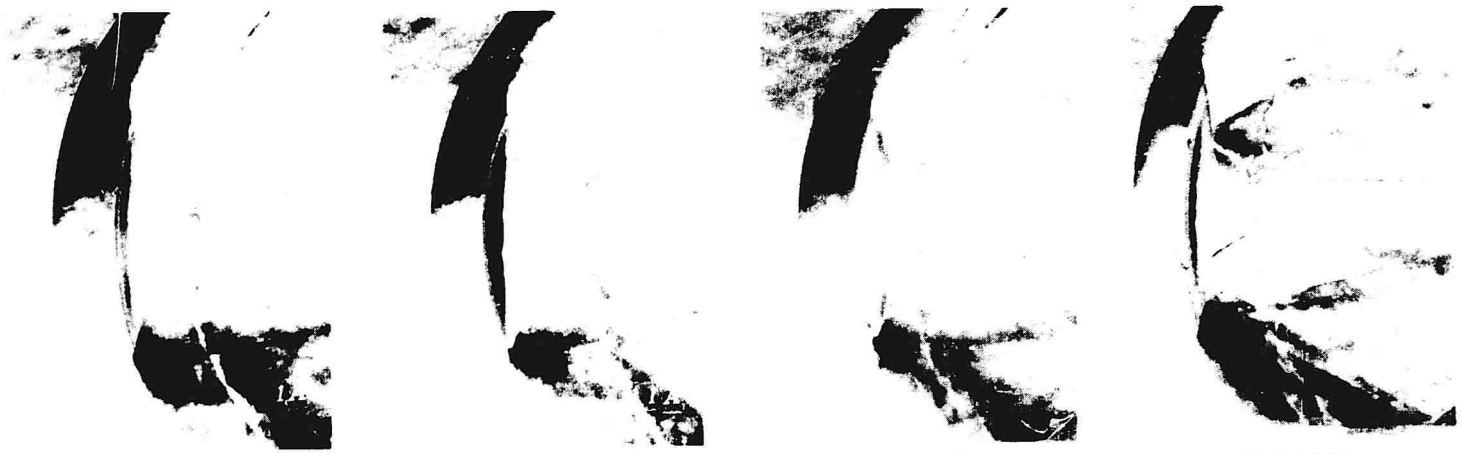

Model 1A Model 11A Model 14A Model 16A

M = 3, $\alpha = 90°$

Fig. 6 Continued

Model 7, $\alpha \approx 20^\circ$

Model 14, with Flaps, $\alpha \approx 0^\circ$

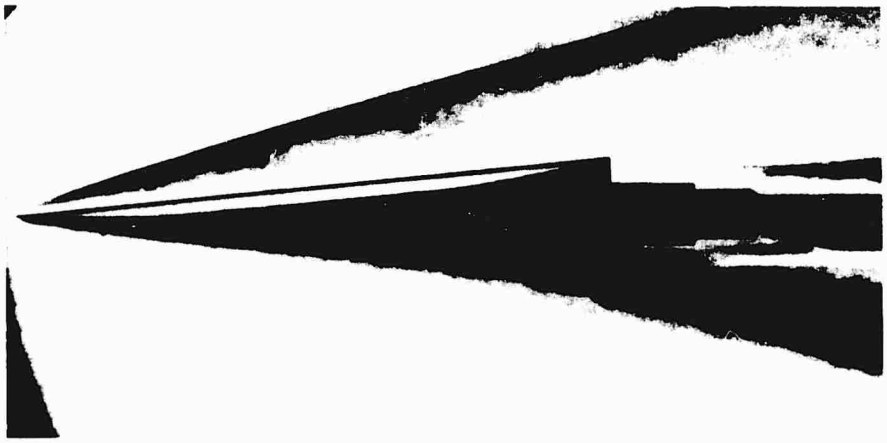

Model 14, without Flaps, $\alpha \approx 0^\circ$

Fig. 6 Concluded

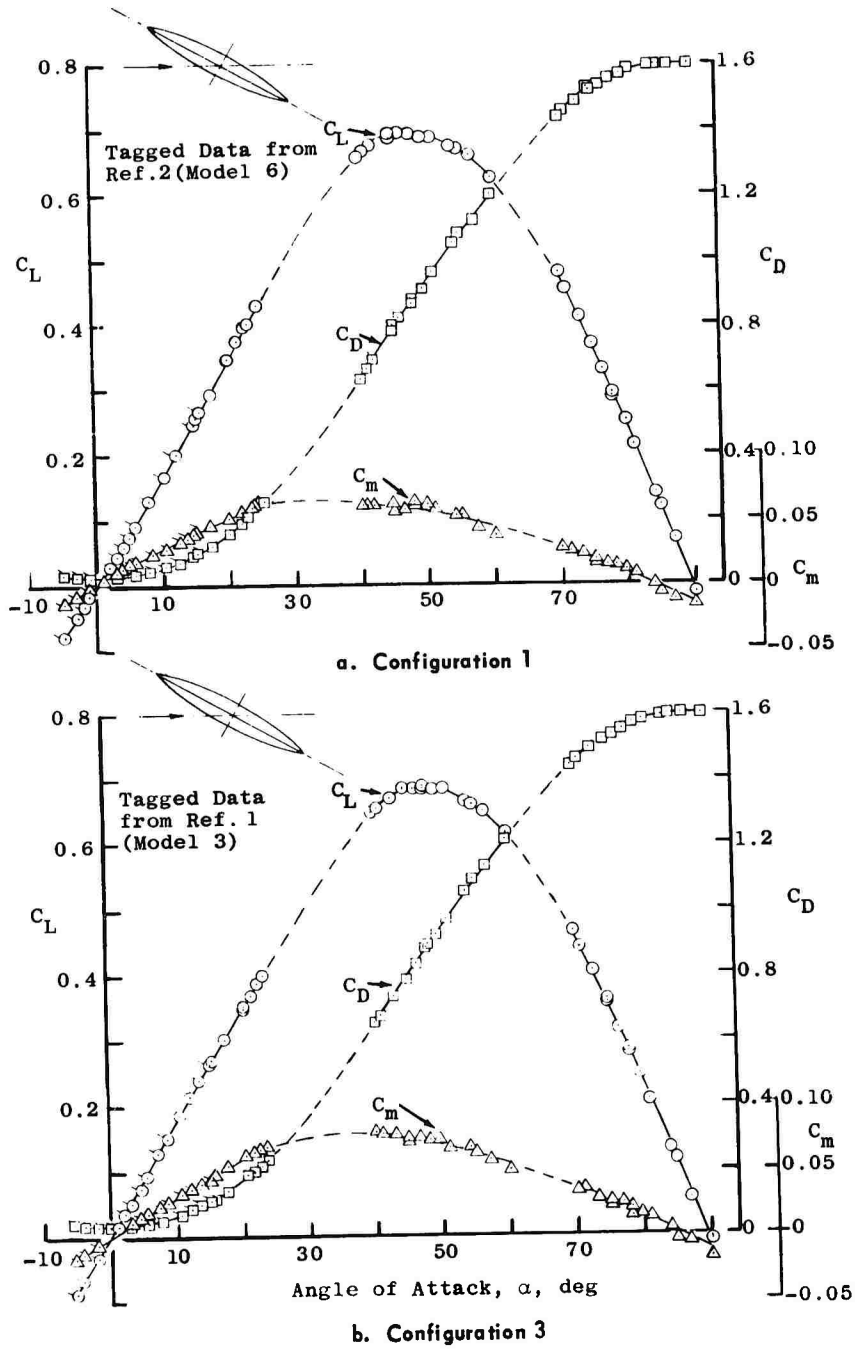

Fig. 7 Lift, Drag, and Pitching-Moment Characteristics at M = 5, α = 0 to 90 deg

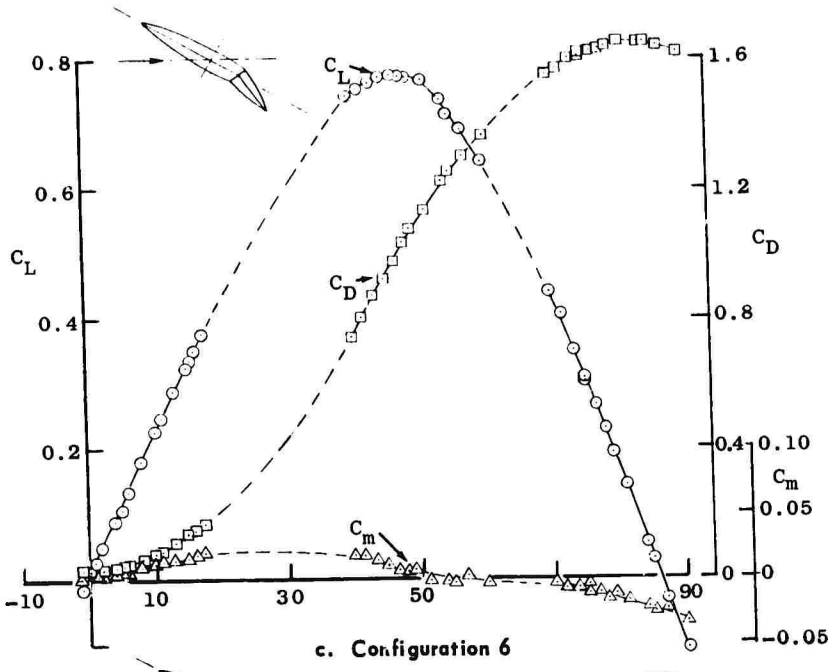

c. Configuration 6

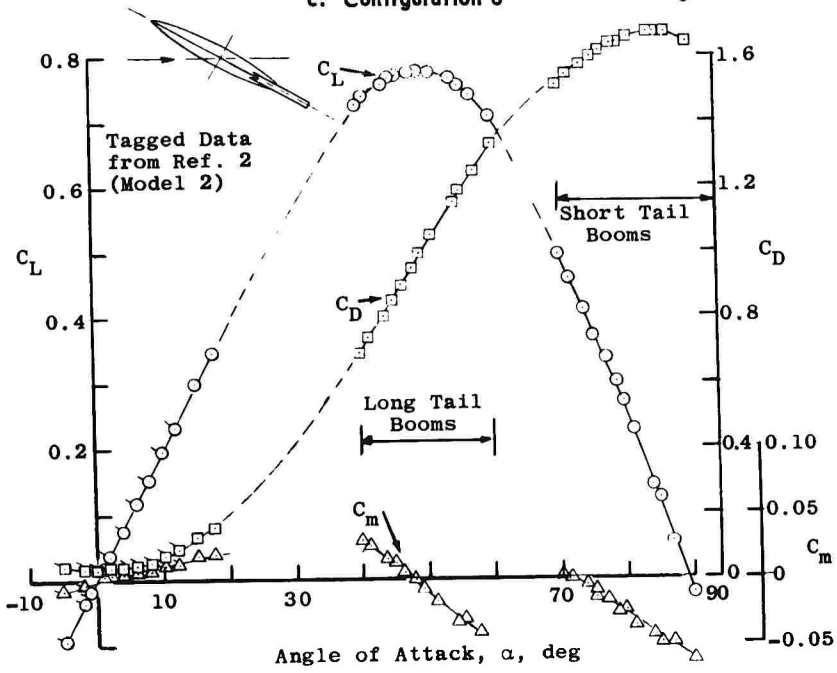

d. Configuration 7

Fig. 7 Continued

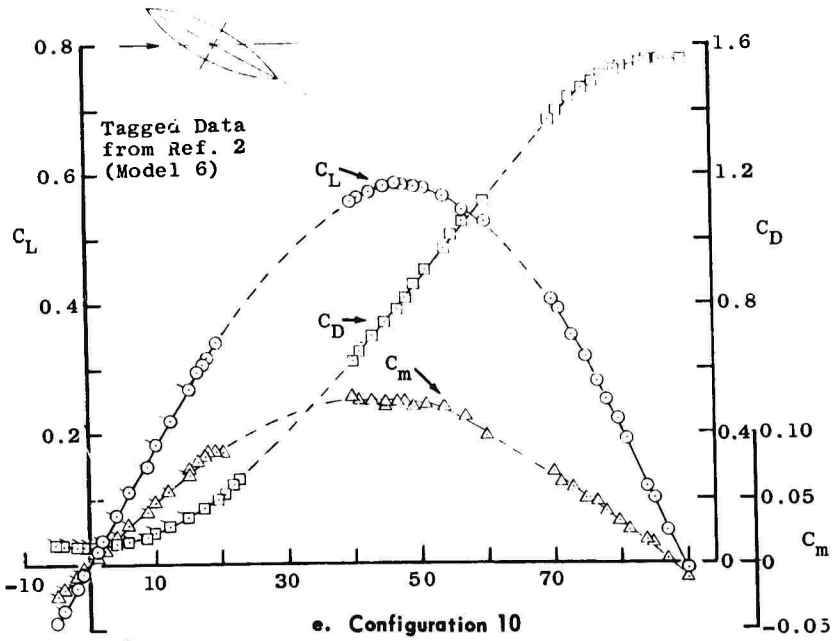

e. Configuration 10

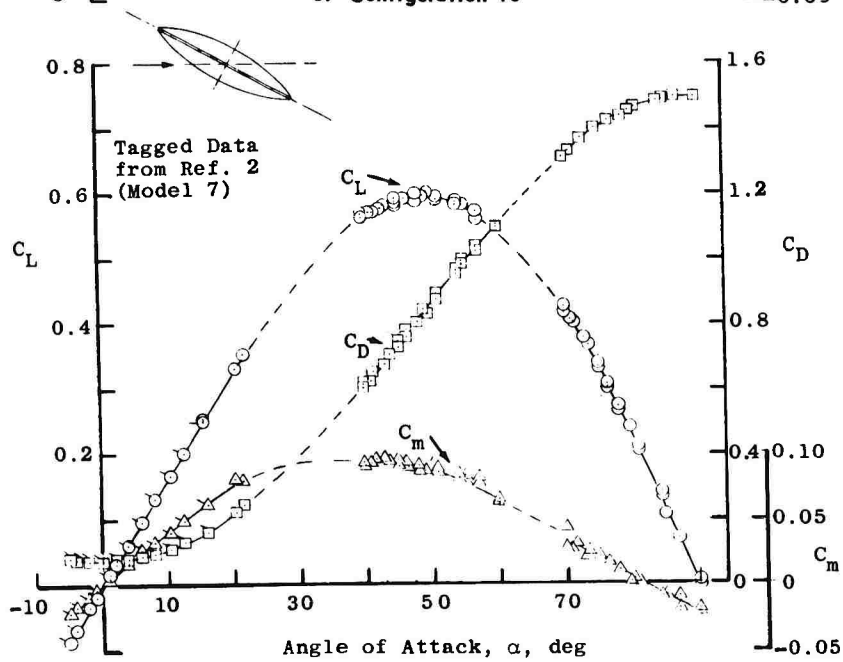

f. Configuration 11

Fig. 7 Continued

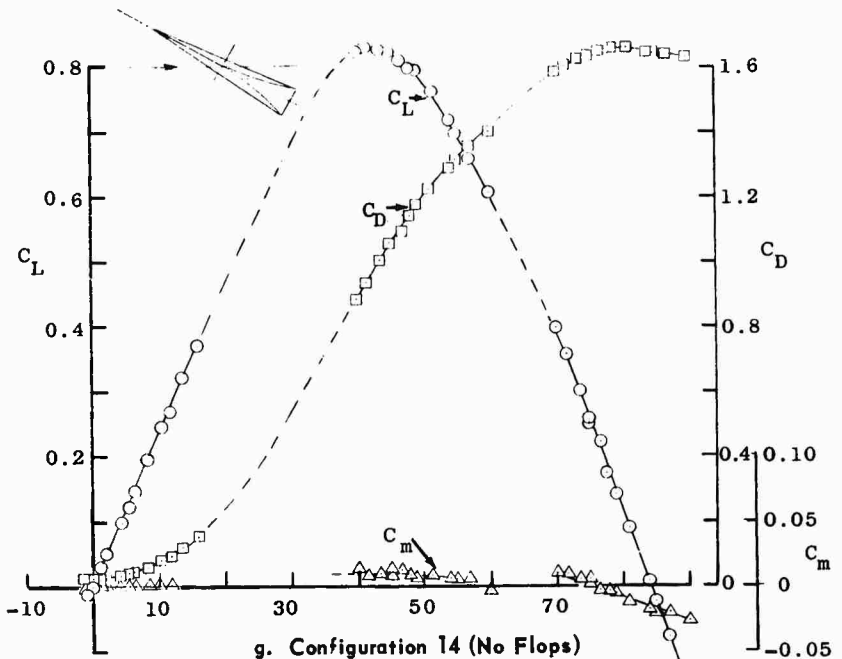

g. Configuration 14 (No Flops)

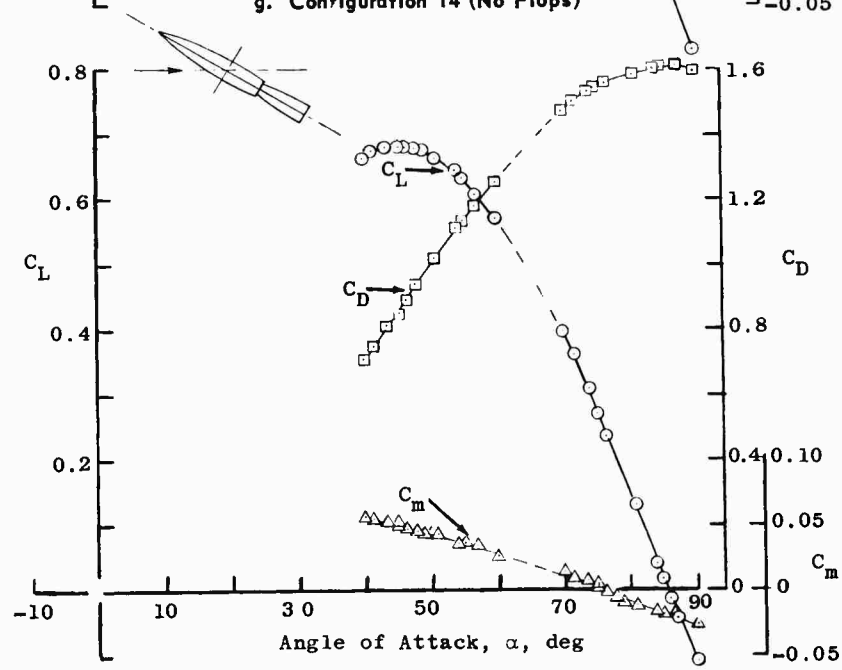

h. Configurotion 16

Fig. 7 Concluded

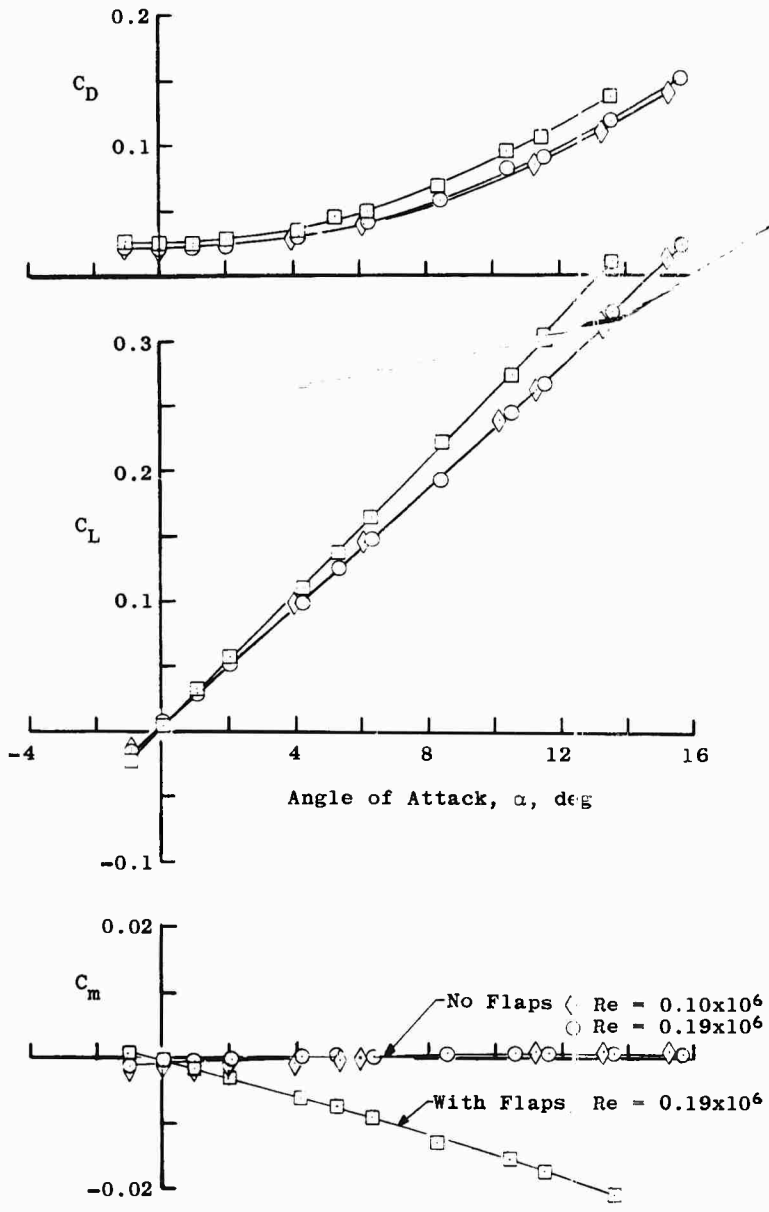

Fig. 8 Lift, Drag, and Pitching-Moment Characteristics for Model 14 at M = 5, α = −1 to 16 deg